1995-01

An Assessment of the Impact of Compressibility on Dynamic Stall

Carr, L.W.

33rd Aerospace Sciences Meeting January 9-12,1995/Reno, Nevada
http://hdl.handle.net/10945/50207

AIAA-95-0779
An Assessment of the Impact of Compressibility On Dynamic Stall

L.W. Carr
Aeroflightdynamics Directorate
US Army ATCOM and
Fluid Mechanics Laboratory Branch
NASA Ames Research Center,
Moffett Field, CA

M.S. Chandrasekhara
Navy-NASA Joint Institute for Aeronautics
Naval Postgraduate School,
Monterey, CA

33rd Aerospace Sciences Meeting
January 9-12, 1995/Reno, Nevada

An Assessment of the Impact of Compressibility on Dynamic Stall

by

L.W. Carr[1]
Aeroflightdynamics Directorate, US Army ATCOM, and
Fluid Mechanics Laboratory Branch
NASA Ames Research Center
Moffett Field, CA 94035-1000

and

M.S. Chandrasekhara[2]
Navy-NASA Joint Institute for Aeronautics
Department of Aeronautics and Astronautics
US Naval Postgraduate School
Monterey, CA 93943

Abstract

The effect of compressibility on dynamic stall is assessed, based on a review of past research in this area. A careful discussion of recent research is presented focusing on both model rotor, and 2-D dynamic stall studies where compressibility effects have been quantified. Examples from the various research efforts are discussed, and detailed analysis of the influence of compressibility on the dynamic stall process is presented. Differences between incompressible and compressible dynamic stall physics are identified, and the role of computation in the modeling of the compressible dynamic stall process is discussed.

Nomenclature

C_l	lift coefficient
$C_{l_{max}}$	maximum lift coefficient
C_m	pitching moment coefficient
C_p	pressure coefficient
$C_{p_{min}}$	peak suction pressure coefficient
c	airfoil chord
f	frequency of oscillation, Hz
k	reduced frequency $= \frac{\pi f c}{U_\infty}$
M_{loc}	local Mach number
M_∞	free stream Mach number
PDI	point diffraction interferometry
Re	Reynolds number based on chord
U_∞	free stream velocity
x,y	chordwise and vertical distance
x/c	nondimensional chordwise distance
z	spanwise distance
α	angle of attack
α_0	mean angle of attack
α_m	amplitude of oscillation
ϕ	phase angle of oscillation
ω	circular frequency, radians/sec
Ω^+	$\frac{\dot{\alpha} c}{U_\infty}$

[1] Group Leader, Unsteady Viscous Flow, Member AIAA.

[2] Associate Director and Research Associate Professor, Assoc. Fellow, AIAA.

1. Introduction

Dynamic stall effects play an important role in defining the flight boundary of helicopters, and the maneuver boundary of fixed-wing aircraft. Research in this area initially focused on global dynamic stall behavior, measuring dynamic lift and pitching-moment excursions caused by the rapid motion of airfoils and wings pushed past the static stall angle. It quickly became clear that dynamic motion changed the character of separation on airfoils. Figure 1(Carr et al[1]) shows the change in the development of stall on an airfoil that occurs due to dynamic motion. This suppression of the wake region, and presence of flow reversal over much of the airfoil without distortion of the surrounding flow, will be important to the analysis of the impact of compressibility on dynamic stall, since this progression of flow reversal from the trailing edge with no external flow distortion formed the basis for much of the benefits that accrue from incompressible dynamic stall.

In fact, it is useful to review the development of dynamic stall as observed in incompressible flow as a basis for showing the effect of compressibility. Figure 2, from a water tunnel test at Reynolds number of 20,000(McAlister and Carr[2]), shows the flow over a oscillating airfoil experiencing dynamic stall. In this case, the airfoil experienced flow reversal near the surface over much of the airfoil before any distortion of the external flow was detected. Figure 3(McAlister and Carr[2]), shows the progression of flow reversal on the airfoil, which is followed by the initiation of the dynamic stall vortex, which moves down the airfoil

as the angle of attack increases. Note the range of angle of attack where flow reversal was observed on the airfoil prior to dynamic stall vortex formation. This same pattern of flow reversal followed by dynamic stall vortex creation and movement can be seen at high Reynolds number, as shown in Figure 4(Carr et al[1]) for tests at Re = 2.5x10^6, where flow reversal is again observed over most of the airfoil prior to dynamic stall onset. This figure shows both the dramatic increase in lift that occurs during dynamic stall at low free-steam Mach numbers, as well as the severe pitching moment excursions that result from dynamic stall. Very large suction peaks accompany the pitching airfoil excursion beyond static stall; Figure 5(McAlister et al[3]) shows that the C_p at the suction peak can approach -30 before separation occurs.

Development of techniques to suppress the formation of the dynamic stall vortex has shown significant potential in incompressible flow. For example, the installation of a leading-edge slat on an oscillating airfoil(Figure 6, from Carr and McAlister[4]) resulted in complete elimination of dynamic stall in the operating range of helicopters(Figure 7, from Carr and McAlister[4]). Boundary layer control through blowing has also been shown to be very effective; Figure 8 from McAlister and Carr[5] demonstrates that dynamic stall can be completely suppressed through use of only moderate blowing along the airfoil surface. Thus, dynamic stall at incompressible flow speeds seems amenable to flow control, is relatively easy to study in the laboratory, and would be a very attractive candidate for application of modern flow control techniques such as neural nets combined with smart materials and/or advanced surface-flow sensors. It will be seen that this picture changes dramatically as the free-stream Mach number increases.

2. The Effect of Moderate Compressibility

Study by helicopter aerodynamicists of airfoil geometry and its influence on dynamic stall loads has suggested that airfoils that stall from the trailing edge in steady flow offer less severe dynamic loads in the dynamic stall environment. This insight has resulted in emphasis on trailing-edge steady-flow stall in design of helicopter rotor airfoils. This trailing-edge stall behavior continues in the dynamic stall environment. Figure 9 from Carr et al[6] shows the flow reversal character of eight airfoils tested in dynamic stall at low free-stream Mach number under identical unsteady conditions; this flow reversal behavior was detected by hot-wire and hot-film anemometer probes located very close to the airfoil surface. Note that five of these airfoils show that flow reversal first appears at the trailing edge, followed by a progression toward the leading edge as the angle of attack increases(the pattern associated with trailing-edge stall). Note that no distortion of the outer flow occurs until this flow reversal appears at the leading edge of the airfoil; in fact, the presence of the dynamic stall vortex is signalled by the appearance of flow reversal at the leading edge of the airfoil. For example, although flow reversal is first detected at 80% chord at 16.7^o angle of attack on the Hughes HH02 airfoil at M_∞ = 0.076, dynamic stall does not occur until α= 21.4^o, when flow reversal is observed at the leading edge of the airfoil. Compare this to the results for the NLR-1, where the dynamic stall vortex appears at α= 17.7^o, coincident with the first appearance of flow reversal on the airfoil(at the leading edge, an example of leading-edge-stall initiated dynamic stall).

Clearly, trailing-edge stall is the dominant flow behavior for these airfoils at low free-stream Mach number. However, flow reversal behavior on these airfoils at M_∞ = 0.30 shows dramatic differences from that observed at M_∞ = 0.10. Figure 10 shows flow-reversal results obtained at M_∞ = 0.30 overlayed on the low Mach number results; virtually all the airfoils which experienced trailing-edge-stall behavior at low Mach number now showed flow reversal to first appear at the leading edge of the airfoils. Note that this also indicates that the dynamic stall vortex has formed at this dramatically lower angle of attack. There are several possible causes for this change; two main possibilities are the increase in Reynolds number and Mach number. For example, these results were obtained in a wind tunnel vented to atmosphere; therefore, increase in Mach number also results in an increase in Reynolds number, suggesting that the change in behavior could be directly associated with boundary layer changes caused by the increase in Reynolds number. To better assess this possibility, consider Figure 11, from Gault[7], where airfoil stall type is mapped as function of Reynolds number and an upper-surface coordinate of the airfoil(which is a measure of curvature at the leading edge). The specified ordinate for the NACA 0012 is marked on this figure; at Re = 1.45x10^6(M_∞ = 0.11 for the McCroskey et al[6] tests), the figure shows the possibility for combined leading edge and trailing-edge stall. This compares favorably with the flow reversal patterns observed in Figure 9. However, at Re = 4.5x10^6(M_∞ = 0.30), the graph shows trailing- edge stall to be the dominant type; thus, increase in Reynolds number increases the probability of trailing-edge stall in steady flow, a pattern contrary to that observed in the experiments on dynamic stall as shown in Figure 9.

A much more likely cause of this abrupt change in stall type can be deduced from Figure 12, from McCroskey et al[8]. This figure documents the maximum local Mach number that appears near the nose of the airfoil during the dynamic stall process as a function free-stream Mach number. Note that at M_∞ = 0.3, the local Mach number shows the flow to be strongly supersonic near the leading edge; Reference 9 shows that M_{loc} = 1.4 is the highest local Mach number that can exist without a strong shock ending the supersonic region. It will be shown that this local supersonic flow region dramatically changes the dynamic stall environment from that observed at incompressible speeds. For example, the maximum C_p that can be attained during dynamic stall is very sensitive to this free stream Mach number. As was shown in Figure 5, the suction peaked near -30 during dynamic stall in incompressible flow. Compare this to Figure 13(McCroskey et al[8]), which shows $C_{p_{min}}$ to be limited to less than -18 at M_∞ = 0.185; Figure 1 shows that $C_{p_{min}}$ is limited to -10 at M_∞ = 0.295(and work at M_∞ = 0.45, presented later in this paper, will show C_p limited to -3.8 before dynamic stall occurred). Thus, a boundary layer that could with-

stand the adverse pressure gradient associated with C_p of -30 that resulted from dynamic stall delay at M_∞ = 0.09 cannot withstand adverse pressure gradients an order of magnitude smaller at M_∞ = 0.40, even though the corresponding increase in Reynolds number should have made the boundary layer more capable of withstanding adverse pressure gradients.

3. Review of Past Research

The results discussed above clearly suggest an effect of compressibility on the dynamic stall process. This is not an isolated example; there are a wide range of studies related to compressibility effects on dynamic stall which offer similar examples(Carr and Chandrasekhara[10]). For instance, increase in $C_{l_{max}}$ due to rapid pitch rate has been demonstrated on fixed-wing aircraft, where the dynamic overshoot of static stall can be significant. Figure 15, based on the work of Harper and Flanigan[11], shows a 90% increase of $C_{l_{max}}$ for a model wing performing a ramp- up maneuver, as rate of pitch increases for tests at M_∞ = 0.10. Figure 16[11] shows the corresponding behavior at progressively higher free-stream Mach numbers; note how quickly the dynamic performance degrades at M_∞ increases. This increase in $C_{l_{max}}$ as pitch rate increases was also observed by Gadeberg[12]. In this case, the maximum lift of a fighter aircraft increased by 30% at M_∞ = 0.18(see Figure 17). This 30% increment of $C_{l_{max}}$ due to pitch-rate was also present at M_∞ = 0.49; however, at M_∞ = 0.49, the $C_{l_{max}}$ at the highest pitch-rate was less than the *static* $C_{l_{max}}$ at M_∞ = 0.18, showing the dramatic impact that compressibility can have on the dynamic overshoot of $C_{l_{max}}$ that occurs during dynamic stall.

The impact of compressibility has also been observed on oscillating airfoils. For example, Figure 18a(Dadone and Fukushima[13]) shows differential pressure coefficients plotted vs phase angle for an airfoil oscillating in pitch at M_∞ = 0.30. This figure shows $C_{p_{min}}$ of -7.0, with smooth variation of the C_p as the cycle progresses. Compare this to Figure 18b, at M_∞ = 0.50; here, the suction pressure drops abruptly as the angle of attack increases, reflecting the separation that occurs on this airfoil during oscillation at this Mach number. Figure 18c, at M_∞ = 0.7, shows the significant change that has occurred at this high Mach number. Note that the leading edge pressures remain unstalled through the high angle of attack part of the cycle; pressure transducers downstream of the leading edge show a loss in suction which the authors[13] suggest is associated with the presence of a shock on this airfoil. Note the drop in $C_{p_{min}}$, even for attached flow, that is shown in this figure.

The effect of Mach number has also been documented on 2-D airfoils performing ramp-type motion, as shown in Figure 19 from Lorber and Carta[14]. The decrease in $C_{l_{max}}$ that occurs as M_∞ increases is clear in this figure, which was obtained for an airfoil operating at Re = 4.0x10^6, M_∞ = 0.4. Thus, the results for an airplane model at Re = 0.9x10^6(Reference 11), a wing in ramp motion at 4x10^6(Reference 14), and a fighter aircraft during flight test at Re= 13.3x10^6(Reference 12) all show the same trend of a decrease in $C_{l_{max}}$ with an increase in Mach number, reinforcing the dominance of Mach number effects over Reynolds number effects in the development of dynamic stall. This relative insensitivity to Reynolds number also implies that regardless of how dynamic stall occurs, the integrated lift may not show major changes in behavior. The sensitivity to Mach number implies that the separation process can be due to significantly different physics and underlying process(shock/boundary-layer interaction, etc), but similar dynamic lift behavior is still obtained.

4. Recent Research on Compressible Dynamic Stall

Past research[15]has suggested that *global* dynamic stall behavior(e.g. lift and pitching moment histories) observed on model rotors can be replicated by 2-D dynamic stall tests. Based on this demonstration of the utility of 2-D tests, two major experimental programs have recently been pursued, focusing on the impact of compressibility on 2-D dynamic stall: one focusing on 2-D representation of dynamic stall effects as observed on model rotors, and one directed towards full-scale Reynolds number and Mach number effects.

4.1. Low Reynolds Number, Compressible Dynamic Stall Studies

The present authors have obtained a considerable body of experimental data on the development of dynamic stall under compressible flow conditions over both an oscillating and a transiently pitching NACA 0012 airfoil at model-rotor-scale Reynolds numbers[16,17,18]. Measurements were made using Point Diffraction Interferometry(PDI), which provides instantaneous density contours in the flow; the PDI images were subsequently processed to yield the surface and global pressure distributions. The study covered a Mach number range of 0.2 to 0.45 and, for the oscillating airfoil, a reduced frequency of 0 to 0.1 depending upon the Mach number; the corresponding chord-based Reynolds number ranged from 360,000 to 810,000. A typical result for the onset of dynamic stall will be discussed below for M = 0.3, k = 0.075 for oscillating motion with $\alpha = 10^o - 10^o \sin\omega t$.

Fig. 20a shows an interferogram at $\alpha = 8.77^o$. In this image, the stagnation point is located at the center of the region on the lower surface near the leading edge where the fringes are nearly circular. As the flow accelerates around the leading edge, the fringes radiate outwards and then gradually turn toward the trailing edge. Near the suction peak, the fringes turn immediately, and return to the surface close to their origin, as can be seen in the picture defining the x/c of maximum suction. As the flow negotiates the pressure gradient here, some fringes are seen to turn downstream parallel to the airfoil surface. Further down the surface, three or four of these fringes abruptly turn towards the surface once more(at about 5-6% chord location), where they the merge with the local boundary layer. The pressure distribution obtained by processing this image is shown on the right(Figure 20). The plateau seen in this image downstream of

the suction peak represents the classical laminar separation bubble which forms as the shear layer separates due to the adverse pressure gradient downstream of the suction peak, undergoes transition and then reattaches. The bubble persists in the flow over a considerable angle of attack range sweep. Eventually at $\alpha = 12.48^o$, the bubble begins to burst. This event is seen as vertical fringes in Fig. 20b, at the the downstream end of the bubble. At $\alpha = 13.24^o$, in Fig. 20c, the images show a full dynamic stall vortex, whose downstream end has already reached x/c = 0.2. This rapid evolution of the dynamic stall vortex with the bursting of the laminar bubble in a very short angle of attack range is typical for the cases studied. It can be seen from the pressure distributions in Figure 20e,f that the flat pressure region extends over the airfoil as the vortex moves down the airfoil, giving rise to enhances lift until it passes the trailing edge of the airfoil.

4.2. Flow at M = 0.45, k = 0.05

For Mach number greater than 0.45, multiple shocks were observed in the flow for both transiently pitching and oscillating airfoil dynamic stall flow. Fig. 21[18] presents an interferogram for M = 0.45, k = 0.05 at α =10 deg. for the oscillating airfoil, where it can be clearly seen that a series of shocks form near the airfoil leading edge. The λ-shocks seen are characteristic of low Reynolds number flow behavior; as the airfoil is pitched, the flow first forms one shock, and as the angle of attack is further increased, more shocks form. Interestingly, the flow does not separate immediately once a shock forms. It seems to be able to withstand the local adverse pressure gradient caused by the shock for a small range of angle of attack before separating. This leads to the conclusion that the shock strength remains small until a larger angle of attack is reached. The pictures for these experimental flow conditions showed that flow separation at the foot of the last shock coincided with formation of the dynamic stall vortex. The cause of the multiple shocks is believed to be due to the interaction of the first shock with the laminar leading edge boundary layer, which seems to introduce a waviness in the boundary layer sufficient for producing the expansion waves and compression waves necessary for the system to sustain itself during a small angle of attack sweep of the airfoil.

Fig. 22[18] shows the global pressure distribution for the above case obtained by processing the PDI image. The leading edge region has been magnified so that the flow variations due to the shocks can be more accurately analyzed. It is clear that the flow becomes supersonic near the surface and that a region of $M > 1$ (the sonic line corresponds to $C_p = -2.76$) which is significantly wider than previously thought exists in the flow. For this condition, five shocks are present which terminate in the sonic line; the outer flow is subsonic. Eventually, a dynamic stall vortex appears, at the foot of the last shock. The x/c location at which this happens is about 0.05 - 0.08, indicating that the dynamic stall vortex does not form at the leading edge.

The above two sections show that the 2D, compressible dynamic stall flow features measured for model-rotor-scale Reynolds numbers are dominated by the presence of the local laminar boundary layer over the airfoil. Since the boundary layer at the chord location of stall onset on a full-scale model or helicopter rotor is likely to be either transitional or turbulent, it was decided to trip the boundary layer in an attempt to simulate these real life conditions. In what follows, some representative results of the study will be presented.

4.3. Flow Over Tripped Airfoil

It is important to recognise that tripping leading-edge-stalling unsteady airfoil flows is inherently difficult and hence very challenging. Since the transition point moves towards the leading edge and the transition length decreases with increasing angle of attack, there is no completely satisfactory method of selecting a trip. Further, the boundary layer thickness changes with Reynolds number of the experiment. This is further complicated by the fact that even in a full-scale system, the state of the boundary layer near the dynamic stall onset location could still be *early-turbulent* and hence, the turbulent flow may not have fully reached equilibrium. With these limitations in mind, several trips were tested. A trip was considered satisfactory if it eliminated the laminar separation bubble, produced larger suction pressure coefficients under the same test conditions and also delayed dynamic stall onset. The most effective trip for fulfilling these criteria was found to have roughly the same height as the laminar boundary layer at the stall onset point. It was made from roughness elements distributed from $0.005 \leq x/c \leq 0.03$. It was glued to the airfoil by a thin lacquer with a combined height of about $45\mu m$.

Fig. 23[18] compares the development of the airfoil peak leading-edge suction as a function of angle of attack for the untripped and tripped airfoil flows at M = 0.3, k = 0.1. It can be seen that the tripped airfoil suction peaks are always higher than that for the untripped airfoil. The C_p value reaches -6.5 just before the formation of the dynamic stall vortex. Further, a delay of about one degree in the angle of attack at which the vortex forms can be seen(14.0° for the tripped case and about 12.8° for the untripped case). Although the vortex convection period over the airfoil does not appear to be different, the delay in onset has resulted in stall delay to higher α for the tripped airfoil; the trends were similar for the case of M_∞ = 0.45. The higher suction peaks meant that the supersonic velocities were higher in the tripped flow.

Fig. 24[18] presents the global pressure coefficient data for $M_\infty = 0.45$, k = 0.05 and $\alpha = 10.0^o$ for the oscillating tripped airfoil. For this case, two shocks were found to be present. Also, the supersonic flow region enveloped by C_p = -2.76 was wider than the corresponding untripped case discussed in Fig. 22. The outer flow was also considerably modified as can be inferred from a comparison of C_p = -1.77 lines. This shows the quantitative differences between the untripped and tripped flows.

A perfect trip would be able to simulate the high Reynolds number test data well. In an effort to assess

the performance of the trip from this point of view, Fig. 25 is drawn. In it, the tripped airfoil surface pressure distribution is compared with the data of McCroskey et al[8] at Re = 3,000,000 along with that for the untripped model-scale airfoil. It can be seen that there is still a noticeable difference between the high Reynolds number data and the tripped low-Reynolds-number airfoil data, although the latter does not have a bubble. This comparison exemplifies the challenges that are faced in extrapolating model-rotor-scale trip data to full-scale-Reynolds-number data.

5. 2-D Dynamic Stall at Flight Mach Number and Reynolds Number

A recent study by Lorber and Carta [19] excellently demonstrates the complex interaction that occurs as Mach number and Reynolds number are increased simultaneously for an airfoil experiencing dynamic stall. In a benchmark experiment performed on a 17-inch-chord airfoil, dynamic stall tests were performed for a range of Mach numbers and Reynolds numbers. Results of these tests documented both the dynamic loads and the flow behavior at the surface of the airfoil during dynamic stall, and offer critical insight into the interactions between compressibility and transition that occurs during compressible dynamic stall at high Reynolds number. Figure 26a, at $M_\infty = 0.20$, Re = 2.0x10^6, shows surface hot-film outputs at various chord locations as this airfoil is put through a ramp motion from 0°-30° angle of attack, as well as the instantaneous pressure distributions at critical points in the flow development. Note first the signals for gages near the leading edge. As the angle of attack increases, transition first appears at x/c =0.302, as an abrupt rise in the hot-film output, corresponding to the increase in heat transfer associated with turbulent flow. As the angle of attack increases, transition moves to x/c = 0.192; the instantaneous pressure distribution associated with this condition is labeled "1". As angle of attack continues to increase, transition moves progressively closer to the leading edge of the airfoil.

Compare these results to those of $M_\infty = 0.30$(Figure 26b). Transition now appears first at x/c = 0.192; as angle of attack increases, transition again moves toward the leading edge. Note that the signal at x/c = 0.026 shows a new pattern just prior to transition - the signal drops before experiencing the rise normally associated with transition to turbulent flow. The authors[19] state that no laminar separation bubble was present in this case, and suggest this is the first evidence of compressibility effects; they indicate that this is an example of compressibility effects on the physics of the boundary layer structure itself. Indeed, this effect is more evident in the $M_\infty = 0.40$ data shown in Fig 26c; the drop in signal strength prior to transition can be seen at point "1" in this figure. The authors found a supersonic region existed on this airfoil which extended past x/c = 0.060, with a maximum local Mach number of 1.27, followed almost immediately by separation of the airfoil flow. The next set of results(Figure 26d) show the character of the flow at $M_\infty = 0.50$. The maximum local Mach number reaches 1.40 at $\alpha = 12°$, and a shock now terminates the supersonic region. The boundary layer starts to separate at the shock at $\alpha = 13.6°$, and the airfoil almost immediately stalls.

5.1. Effect of Free-Stream Turbulence

Thus, 2-D dynamic stall research, both at model- and at full-scale Reynolds numbers, shows the strong effect that compressibility has on the dynamic stall process. There are clear differences between the model-scale and full-scale 2-D results; the next step would seem to be to compare the model-scale 2-D data to model-scale rotor data, and to make the corresponding comparisons for full scale. Model-rotor–scale tests have recently been performed at full-scale Mach number by Lorber[20]. After review of these model- rotor results, Lorber[21] found that the airfoil stall that is observed on the model rotor more closely resembles full-scale 2-D dynamic stall data than model scale 2-D dynamic stall. Lorber suggests that one possible contributor to this disparity is the influence of rotor-induced "free-stream" turbulence. Conventional laminar separation bubble behavior does not seem to appear on the model rotor, possibly because the "free-stream" turbulence is so high that the laminar separation bubble is abruptly closed. Therefore, transition effects are present on the model-rotor, but the effects mimic transition at much higher Reynolds number because of the high turbulence level in the surrounding flow. Studies of airfoil stall where laminar/transitional effects are important show dramatic increases in $C_{l_{max}}$ as free-stream turbulence is increased. For instance, Figure 27 from Hoffman[22] shows the impact of major free stream turbulence on the $C_{l_{max}}$ of a NACA 0015 airfoil at Re = 250,000. As can be seen from the figure, the airfoil stall characteristics change dramatically as the free-stream turbulence is increased.

There are concerns about effective tripping of the airfoil at model-scale Reynolds numbers, where any trip placed on the surface of the small model-rotor airfoil may result in interaction between the trip and the inviscid flow, rather than simply creating an instability within the boundary layer as occurs at larger scale. In addition, the fact that 2-D dynamic stall tests performed at the same Reynolds number and Mach number as model-rotor tests do not match the character of the stall on the model rotor suggests the presence of additional physics that is not presently being properly included. One possible way to address this issue would be to introduce high free stream turbulence(HFST) into both computations and experiments as a practical way to more accurately reproduce the helicopter rotor environment. This complex combination of flow- and airfoil-unsteadiness indicates the difficulties faced by engineers and scientists hoping to develop insight and technology directed toward control of dynamic stall. When this HFST condition is combined with the effects of compressibility, it is clear that low-speed, low-Reynolds number studies are not extendable to the full-scale rotor without major effort to include these effects.

6. Calculation of Compressibility Effects on Dynamic Stall

Although there has been significant research effort focused on calculation of dynamic stall using Navier-Stokes-equation representation of the unsteady flow field, relatively few calculations have focused specifically on the effect of compressibility on the dynamic stall process; even these are spread over a wide range of Reynolds numbers. Very low Reynolds number (Re = 5000) calculations were performed by Sankar and Tassa [23] which showed that the dynamic stall vortex was delayed at $M_\infty = 0.4$ when compared to that at $M_\infty = 0.2$. A similar result has also been obtained by Choudhuri and Knight[24] at a higher Reynolds number of 100,000. These grid-resolved calculations were able to capture the shock that forms at the higher Mach number as well. The calculations also showed that increasing the Reynolds number at a constant Mach number caused earlier onset of local flow reversal and hence stall inception. It is of interest to note that experimental results discussed earlier show that the dynamic stall process is promoted as the Mach number is increased under compressible flow conditions.

Visbal[25] computed the effects of compressibility over a ramping NACA 0015 airfoil using unsteady turbulent Navier-Stokes-equations computations. These moderately high Reynolds number(200,000) calculations showed a supersonic flow region near the nose of the airfoil. Results at $M_\infty = 0.4$, $\Omega^+ = 0.045$, Re = 1 x 10^6 are presented in Figure 28[25], which shows that the supersonic region is terminated by a normal shock.Visbal attributes the shock/boundary-layer interaction as being a mechanism for dynamic stall delay. The observation of a laminar bubble in the experiments of Chandrasekhara and Carr[18] at a similar Reynolds number showed the presence of the multiple shocks as has already been discussed. The complexity of the problem limits any direct comparison between experiments and computations under these conditions; however, the same impact of compressibility was also determined by Visbal, as illustrated in Figure 29, where C_l *vs* α is presented for a range of free-stream Mach numbers, showing the progressive decrease in stall angle associated with increase in Mach number. Ekaterinaris[29] also addressed the effect of compressibility for an SSC-A09 airfoil section at Reynolds number of 2 x 10^6, once again using Navier-Stokes equation modeling of the dynamic stall process. Figure 30 shows a comparison between calculation and the experiment of Lorber and Carta[19] which shows the decrease in dynamic stall angle that occurs as free-stream Mach number is increased. Geissler[27] in his computations also found the presence of a supersonic region. He also observed that the fully turbulent calculations showed a higher stall inception angle when compared to the experiments of Chandrasekhara and Carr[18], pointing to the role of transition on the problem. Srinivasan et al[28] studied the dependence of the results on turbulence model. The results were found to be very sensitive to the model used, with none of the models giving full agreement with the data of McCroskey et al[8]. VanDyken et al[29] show that to obtain reasonable agreement with the data of Chandrasekhara and Carr[16], it is necessary to include the influence of transition.

This section shows that matching the 2-D experimental results on compressibility effects on dynamic stall is still a challenge. Such an effort for the model rotor is even more formidable, since the effects of rotor induced turbulence needs to be included. Thus, much work still needs to be done in the area of experiments and computations to produce results of practical interest.

7. Discussion

The results reviewed in this paper show that assessing the impact of compressibility on dynamic stall is a very difficult task to perform quantitatively. However, several aspects of the problem have been qualitatively identified. For instance, it is now clear that increase in Reynolds number at incompressible flow velocity will not properly represent dynamic stall at flight Reynolds number and Mach number. In a similar way, increase in Mach number at low Reynolds number does not capture the change in flow physics that results from lift-induced compressibility at high Reynolds number. The 2-D character of the flow at flight Mach and Reynolds number has been experimentally determined(Lorber and Carta[19]), but only for the isolated and singular case of the SSC-A09 airfoil; documentation of the dynamic behavior of other airfoils will require similar tests. Compressibility effects have been observed for several airfoils at lowe. Mach number[8], but the effects are limited by the relatively low free-stream Mach number of that test. The performance of the NACA 0012 airfoil has been explored at model-rotor-scale conditions[18], but no test has fully bridged the gap from model to full scale.

The reality of the research environment for the foreseeable future is that there will not be many opportunities for tests at flight Mach numbers and Reynolds numbers. Therefore, the most probable approach to quantification of the effect of airfoil shape, flow control, etc, on dynamic stall in compressible flow will be on model-scale helicopter rotors. At the same time, future developments in flow control, smart materials, surface sensors for detection of stall precursors, etc, will most likely be developed in the laboratory at low Mach number and Reynolds number, on fixed airfoils, reinforcing the need for techniques to bridge the gap between laboratory and flight. As shown above, compressibility effects must be considered before any flow-control technique can be proposed for application to the rotor. This does not mean that full-scale Mach and Reynolds numbers must be obtained. Nor does it mean that transition, and the difficulties associated with modeling of separation bubbles necessarily need to be included. Rather, the focus may best be placed on modeling of model-Reynolds-number, fully turbulent flow, in a flow with high free-stream turbulence representing the flow that occurs on airfoils in the helicopter rotor environment It should be possible to develop turbulence model. that can bridge the gap between this model-scale turbulent flow and full-scale turbulent flow on airfoils. When this bridge is built, prediction of dynamic stall at flight Mach numbers and Reynolds numbers could

be made based on model-scale compressible studies, thus allowing helicopter aerodynamicists the opportunity to quantitatively optimize rotor behavior through the use of model rotor experiments.

8. Concluding Remarks

Compressibility effects have been shown to play a critical part in the dynamic stall of helicopter rotor blades, both on model rotors and full-scale helicopters. Research quantifying the influence of compressibility has been performed in two dimensions, both at model-, and at full-scale Reynolds numbers, but attempts at extension of these 2-D results to the rotating environment has shown that not all the physics of the rotating environment has been captured in research conducted to date. The survey of past research performed in this review has shown that compressibility must be included in any study of dynamic stall associated with the helicopter rotor, and that increase in Reynolds number without inclusion of compressibility effects will definitely not capture the stall-generating physics that appear on the helicopter rotor in flight.

At the same time, there is evidence that properly performed 2-D tests can reasonably represent the developing dynamic stall flow field, especially when the high free-stream turbulence level that occurs in the helicopter rotor environment is reproduced in the 2-D non-rotating environment. It is thus recommended that future 2-D dynamic stall tests should consider inclusion of high levels of free stream turbulence. In order to quantify the dynamic stall behavior, tests should match the airfoil geometry that has been used in existing model and full-scale rotor tests. In this way, truly quantitative comparisons between 2-D and rotor tests can be performed. Once this quantitative comparison can be made, evaluation of control techniques can be performed in the non-rotating environment with higher probability that the results will apply in flight.

Acknowledgements

The work was supported by ARO-MIPR-125-93 to the Naval Postgraduate School and was monitored by Dr. T.L. Doligalski. Additional support was received from the U.S. AFOSR, which was monitored by Maj. D.B. Fant. The work was carried out in the Fluid Mechanics Laboratory Branch of NASA Ames Research Center. The encouragement of Dr. S.S. Davis, Chief, FML Branch, the able assistance of Dr. M.C. Wilder while performing the experiments, the support of Mr. J.D. Loomis in the conduct of experiments and the interferogram image processing support of Ms. S.Nado are greatly appreciated.

9. References

1. Carr, L.W., McAlister, K.W., and McCroskey, W.J., "Analysis of the Development of Dynamic Stall Based on Oscillating Airfoil Experiments", *NASA TN D-8382*, Jan. 1977.

2. McAlister, K.W., and Carr, L.W., "Water Tunnel Visualizations of Dynamic Stall", *Jl. of Fluids Engineering*,Trans. ASME, Vol. 101, No. 2, Sep. 1979, pp. 376-380.

3. McAlister, K.W., Carr, L.W., and McCroskey, W.J., "Dynamic Stall Experiments on the NACA 0012 Airfoil", *NASA TP-1100*, 1978.

4. Carr, L.W., and McAlister, K.W., "The Effect of a Leading-Edge Slat on the Dynamic Stall on an Oscillating Airfoil", *AIAA-83-2533*, AIAA/AHS Aircraft Design, System and Operations Meeting, Oct. 17-19, 1983, Fort Worth, TX

5. Results of Unpublished Experiment

6. Carr, L.W., McCroskey, W.J., McAlister, K.W., Pucci, S.L., and Lambert, O., "An Experimental Study of Dynamic Stall on Advanced Airfoil Sections, Volume 3: Hot-Wire and Hot-Film Measurements", *NASA TM 84245*, Dec. 1982.

7. Gault, D.E., "A Correlation of Low-Speed, Airfoil-Section Stalling Characteristics With Reynolds Number and Airfoil Geometry", *NACA TN 3963*, Mar. 1957.

8. McCroskey, W.J., McAlister, K.W., Carr, L.W., Pucci, S.L., Lambert, O., and Indergand, R.F.(1981), "Dynamic Stall on Advanced Airfoil Sections", *Jl. of American Helicopter Society*, Jul. 1981, pp. 40-50.

9. Pearcey, H.H., "Some Effects of Shock-Induced Separation of Turbulent Boundary-Layers in Transonic Flow Past Aerofoils", in Boundary Layer Effects in Aerodynamics, Proceedings of The Symposium held at N.P.L., London, England, April 1, 1955.

10. Carr, L.W., and Chandrasekhara, M.S., "Research on Compressible Dynamic Stall", To appear in *Progress in Aerospace Sciences*, 1995.

11. Harper, P.W., and Flanigan, R.E., "The Effect of Rate of Change of Angle of Attack on the Maximum Lift of a Small Model", *NACA TN 2061*, 1950.

12. Gadeberg, B.L., "The Effect of Rate of Change of Angle of Attack on the Maximum Lift Coefficient of a Pursuit Airplane", *NACA TN 2525*, October 1951.

13. Fukushima, T., and Dadone, L.U.,"Comparison of Dynamic Stall Phenomena for Pitching and Vertical Translation Motions", *NASA CR-2793*, December 1976.

14. Lorber, P.F., and Carta, F.O., "Airfoil Dynamic Stall at Constant Pitch Rate and High Reynolds Number", *Jl. of Aircraft*, Vol. 25, No. 6, Jun. 1988, pp. 548-556.

15. Ham, N.D., and Garelick, M.S., "Dynamic Stall Considerations in Helicopter Rotors" *Jl. of American Helicopter Society*, Vol. 13, No. 2., Apr. 1968, pp. 49-55.

16. Carr, L.W., Chandrasekhara, M.S., and Brock, N.J., "A Quantitative Study of Unsteady Compressible Flow on an Oscillating Airfoil", *Jl. of Aircraft*, Vol. 31, No. 4, Aug. 1994, pp. 892-898.

17. Chandrasekhara, M.S., Wilder, M.C., and Carr, L.W., "Interferometric Investigations of Compressible Dynamic Stall Over a Transiently Pitching

Airfoil", *AIAA Jl.*, Vol. 32, No. 3, Mar. 1994, pp. 586-593.

18. Chandrasekhara, M.S., and Carr, L.W., "Compressibility Effects on Dynamic Stall of Oscillating Airfoils", AGARD 75th Fluid Dynamics Panel Meeting on "Aerodynamics and Aeroacoustics of Rotorcraft", Berlin, Germany, Oct. 10-13, 1994, pp. 3.1 - 3.15.

19. Lorber, P.F., and Carta, F.O., "Unsteady Transition Measurements on a Pitching Three-Dimensional Wing", presented at *the Fifth Symposium on Numerical and Physical Aspects of Aerodynamic Flows*, Long Beach, CA, Jan. 13-15, 1992.

20.Lorber, P.F., Stauter, R.C., Haas, R.J., Anderson, T.J., Torok, M.S., and Kohlhepp, F.W., "Techniques for Comprehensive Measurement of Model Rotor Aerodynamics", *AHS 50th Annual Forum*, Washington, D.C., May 11-14, 1994.

21. Lorber, P.F., "Private Communication".

22. Hoffman, J.A., "Effects of Freestream Turbulence on the Performance Characteristics of an Airfoil", *AIAA Jl.*, Vol. 29, No. 9, Sep. 1991, pp. 1353-1354.

23. Sankar, N.L., and Tassa, Y., "Compressibility Effects on Dynamic Stall of a NACA 0012 Airfoil", *AIAA Jl.*, Vol. 19, No. , May 1981, pp. 557-568.

24.Choudhuri, P.G., and Knight, D., "Effects of Compressibility, Pitch Rate, and Reynolds Number on Unsteady Incipient Boundary Layer Separation Over a Pitching Airfoil", *AIAA-95-0782*, 33rd AIAA Aerospace Sciences Meeting and Exhibit, Reno, NV, Jan. 9-12, 1995.

25. Visbal, M.R., "Dynamic Stall of a Constant-Rate Pitching Airfoil", *Jl. of Aircraft*, Vol. 27, No. 5, May 1990, pp. 400-407.

26. Ekaterinaris, J.A., "Compressible Studies on Dynamic Stall", *AIAA-89-0024*, 27th Aerospace Sciences Meeting, Reno, NV, January 9-12, 1989.

27. Geissler, W., and Sobieczky, H., "Dynamic Stall Control by Variable Airfoil Camber", AGARD Symposium on Aerodynamics and Aeroacoustics of Rotorcraft, Oct. 10-14, 1994, Berlin, Germany

28. Srinivasan, G.R., Ekaterinaris, J.A., and McCroskey, W.J., "Dynamic Stall of an Oscillating Wing, Part 1: Evaluation of Turbulence Models", *AIAA-93-3403*, AIAA 11th Applied Aerodynamics Conference, Monterey, CA, August 9-11, 1993.

29. Van Dyken R.D.,Ekaterinaris, J.A., Chandrasekhara, M.S., and Platzer, M.F., "Analysis of Compressible Steady and Oscillatory Airfoil Flows at Transitional Reynolds Numbers", *AIAA-94-2255*, AIAA 25th Fluid Dynamics Conference, Colorado Springs, CO, Jun. 20-23, 1994.

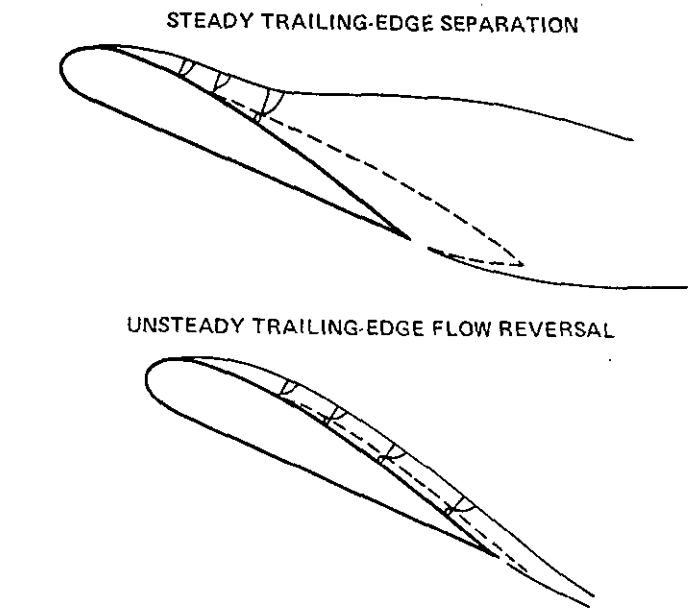

Figure 1. Boundary Layer Separation and Stall of an Airfoil in Steady and in Unsteady Flow(from Reference 1).

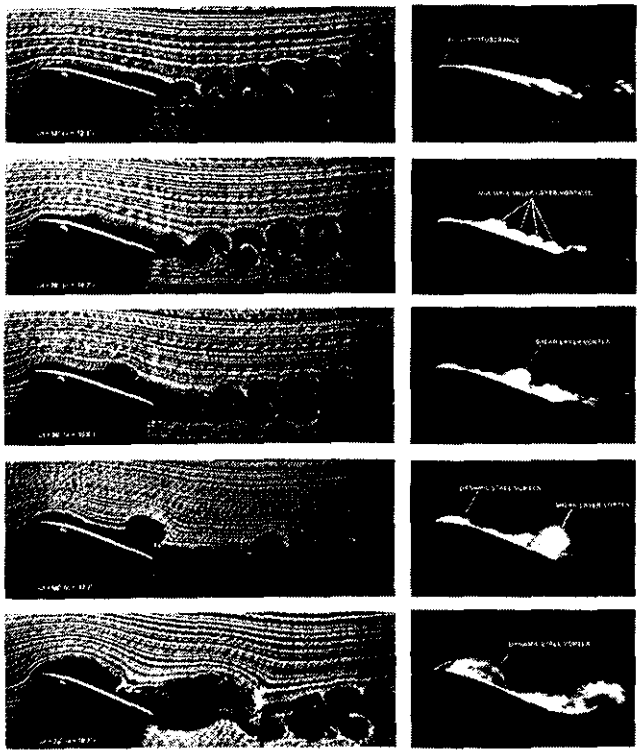

Figure 2. Dynamic Stall of an Oscillating Airfoil in a Water Tunnel at Re = 20,000(from Reference 2).

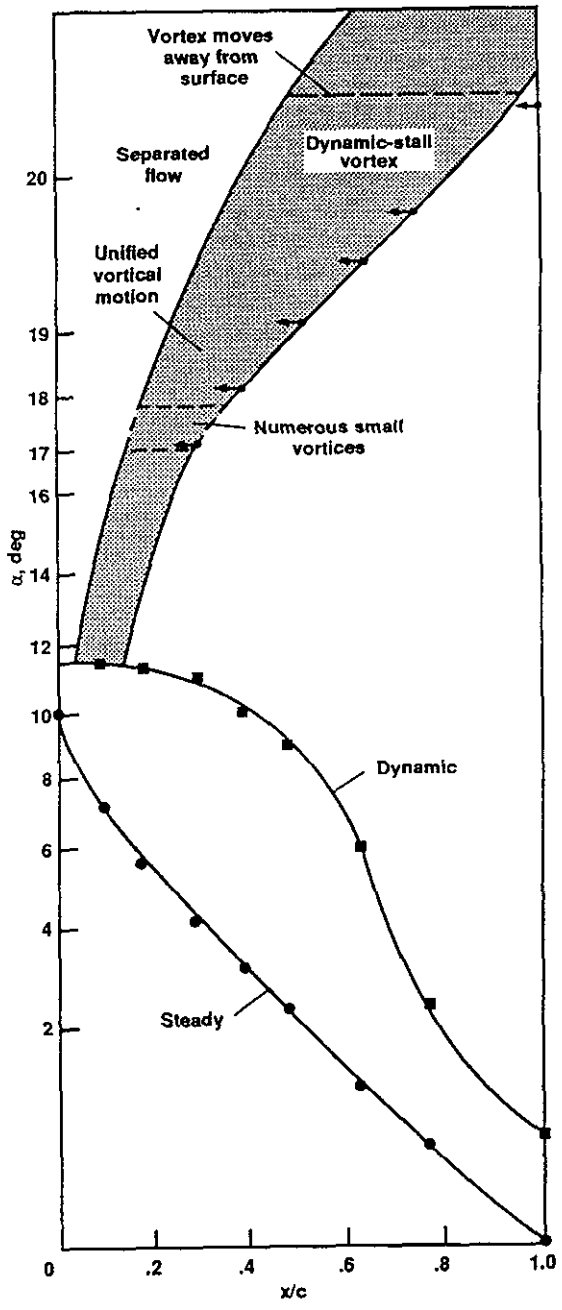

Figure 3. Progress of Flow Reversal and Development of the Dynamic Stall Vortex on and Oscillating Airfoil in a Water Tunnel at Re = 20,000(from Reference 2).

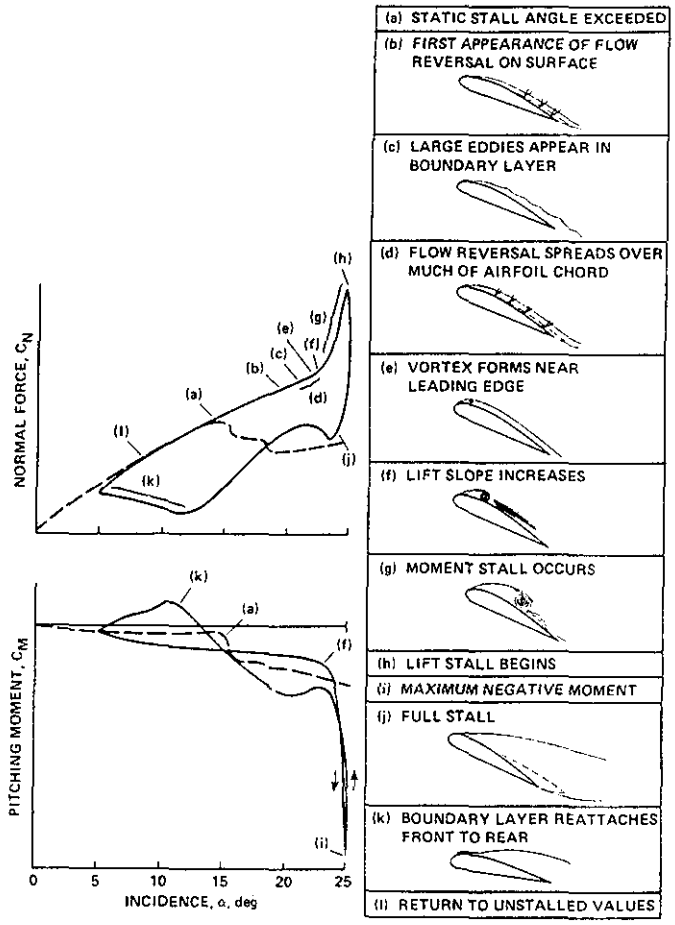

Figure 4. Development of Dynamic Stall on an Oscillating Airfoil at Re = $2\text{x}10^6$, M_∞ = 0.09(from Reference 1).

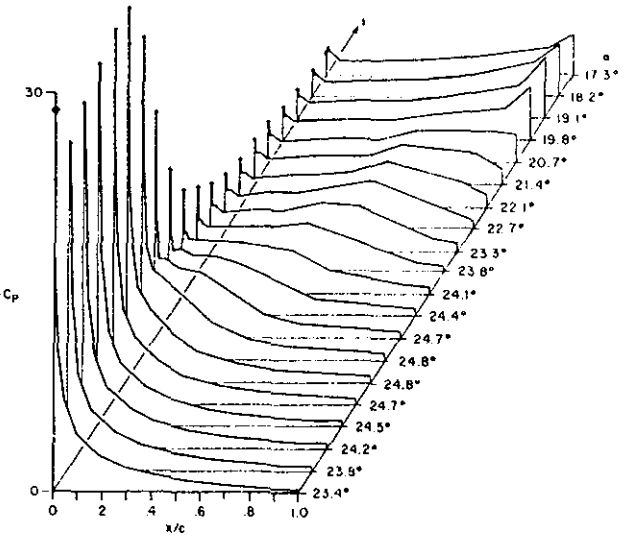

Figure 5. Instantaneous Pressure Distributions Measured on an Oscillating Airfoil at M_∞ = 0.09(from Reference 5).

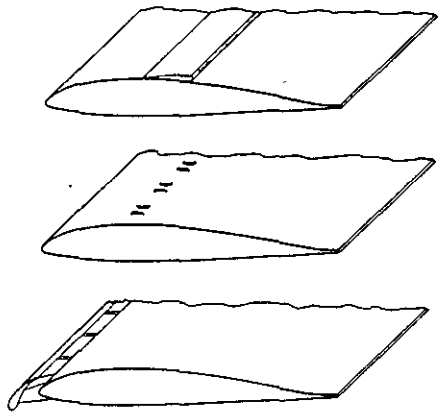

Figure 6. Airfoil Modifications Tested in Effort to Suppress Dynamic Stall Vortex Formation(from Reference 4).

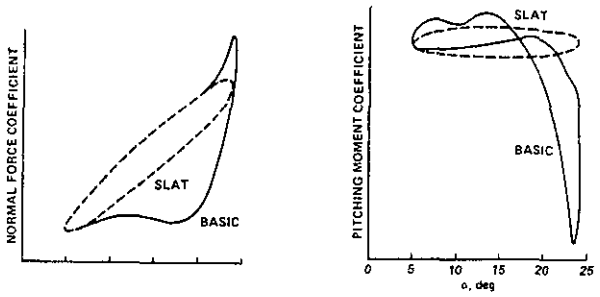

Figure 7. Effect of Slat on Normal Force and Pitching Moment of Oscillating Airfoil(from Reference 4).

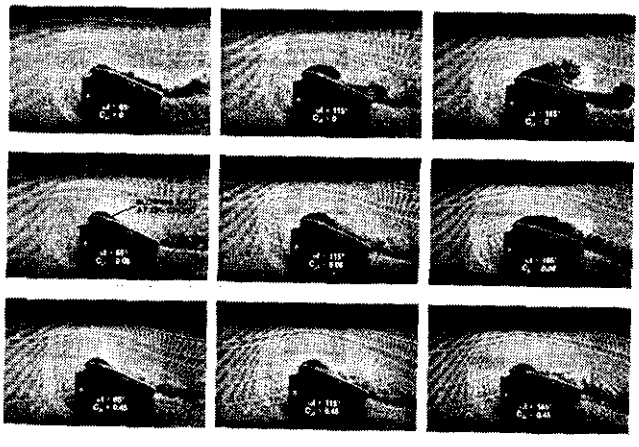

Figure 8. Effect of Tangential Blowing on Development of Dynamic Stall on an Oscillating Airfoil(unpublished experimental results).

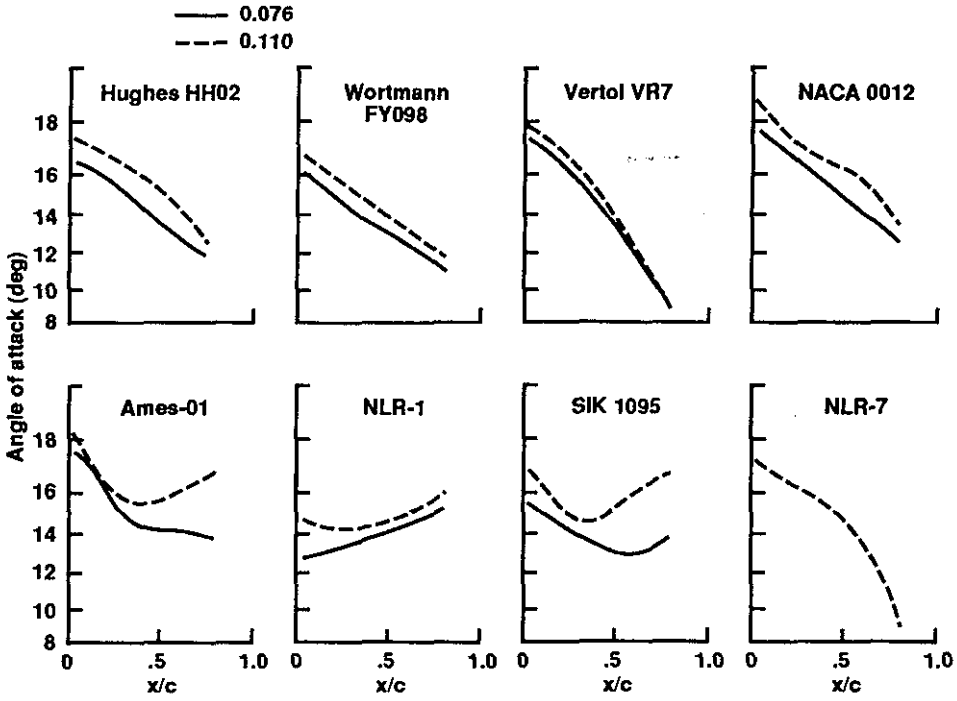

Figure 9. Flow Reversal Characteristics of Eight Airfoils Experiencing Dynamic Stall at Low Free-Stream Mach Number[Re = 1.45×10^6 at M = 0.11](from Reference 6).

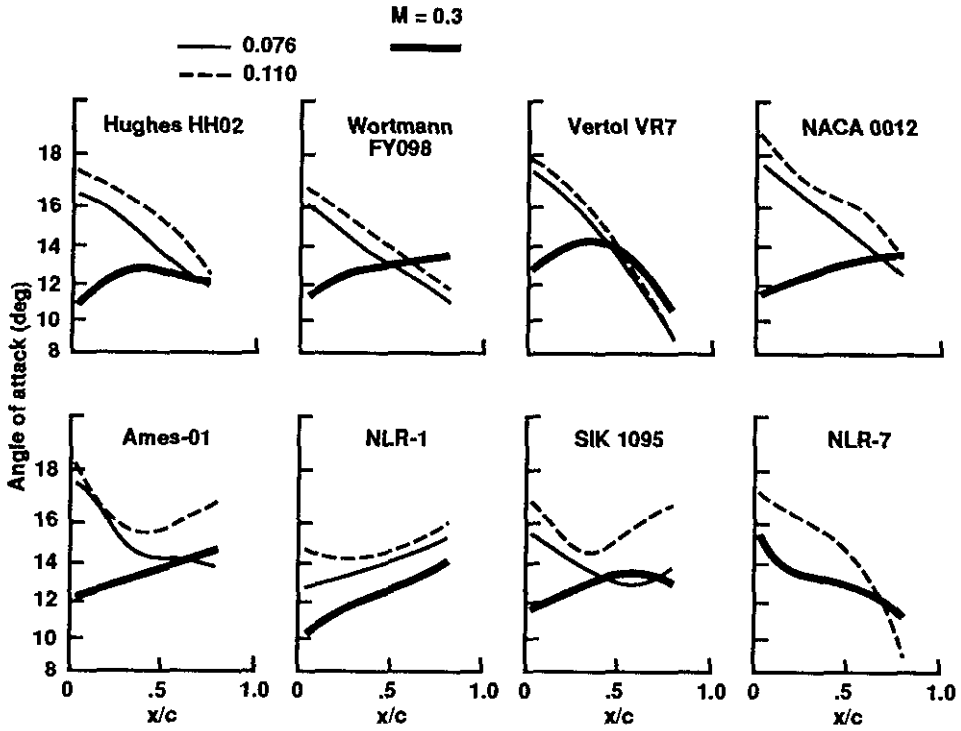

Figure 10. Flow Reversal Characteristics of Eight Airfoils Experiencing Dynamic Stall at Moderate Free-Stream Mach Number[Re = 4.0×10^6 at M = 0.30](from Reference 6).

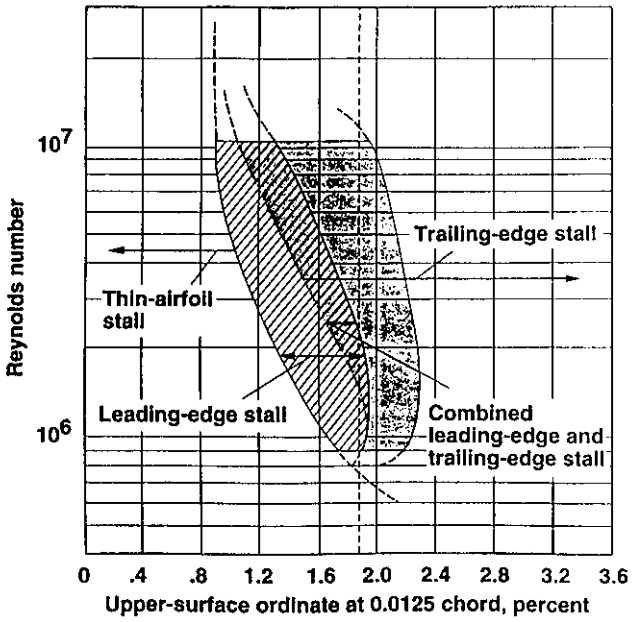

Figure 11. Low-Speed Stalling Characteristics of Airfoil Sections Correlated with Reynolds Number and Surface Ordinate(from Reference 7).

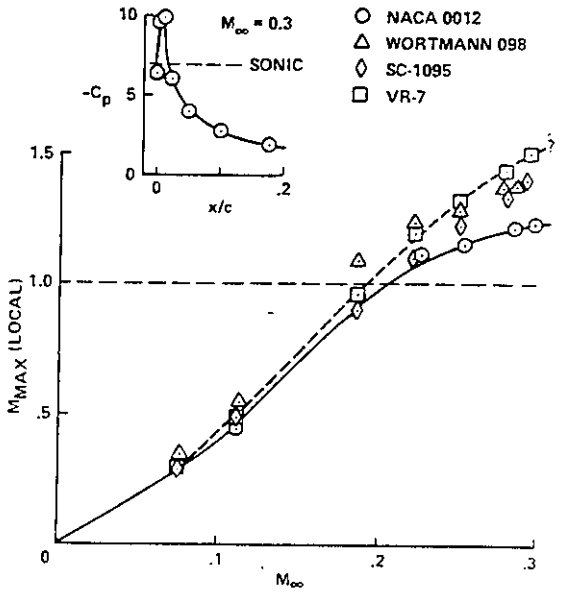

Figure 12. Variation of Maximum Local Mach Number on Oscillating Airfoil as Function of Free-Stream Mach Number(from Reference 8).

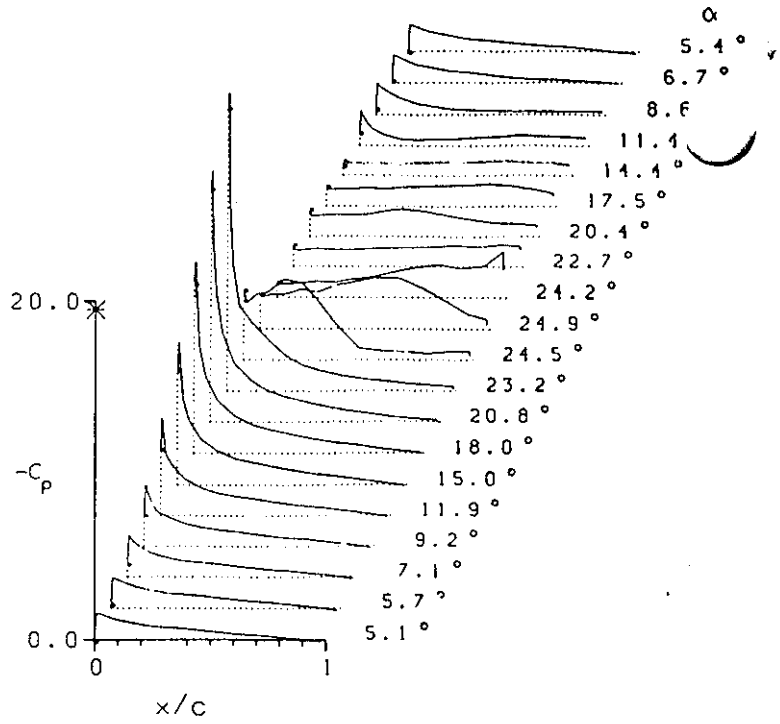

Figure 13.Instantaneous Pressure Distributions for Airfoil Oscillating in Angle of Attack at $M_\infty = 0.185$(from Reference 8).

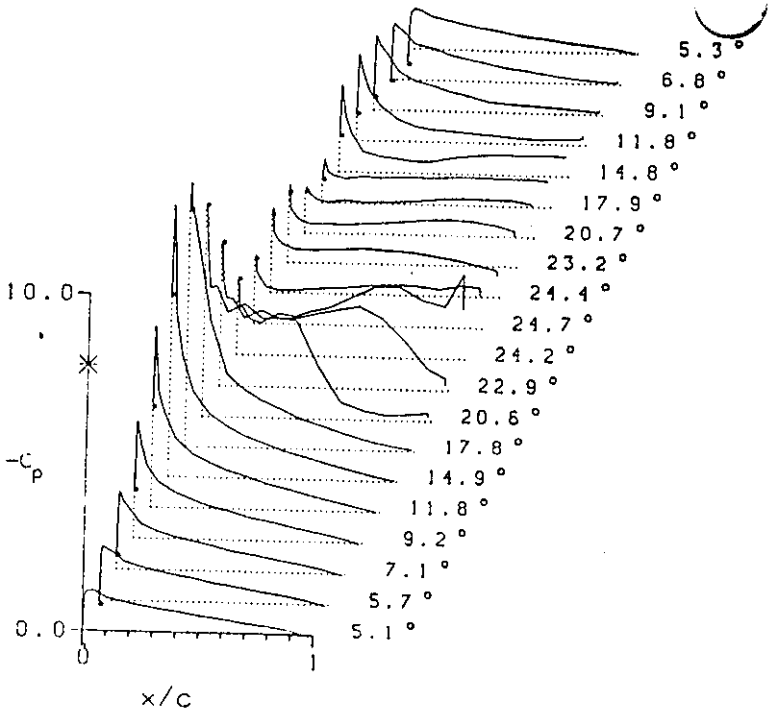

Figure 14.Instantaneous Pressure Distributions for Airfoil Oscillating in Angle of Attack at $M_\infty = 0.295$(from Reference 8).

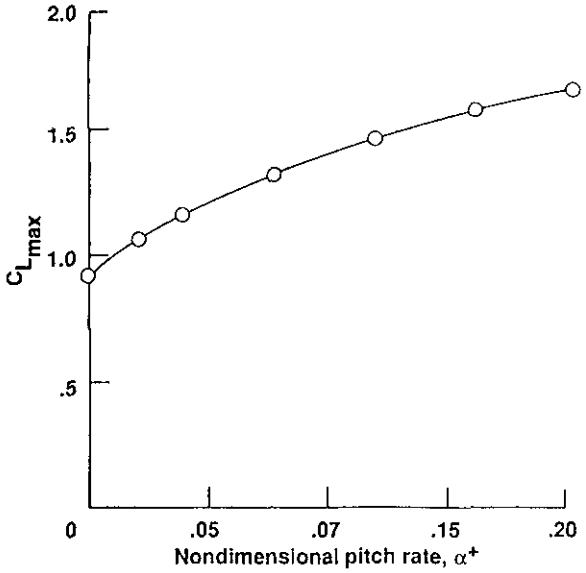

Figure 15. Effect of Pitch Rate on Maximum LIft of an Model Aircraft Wing at $M_\infty = 0.10$(from Reference 11).

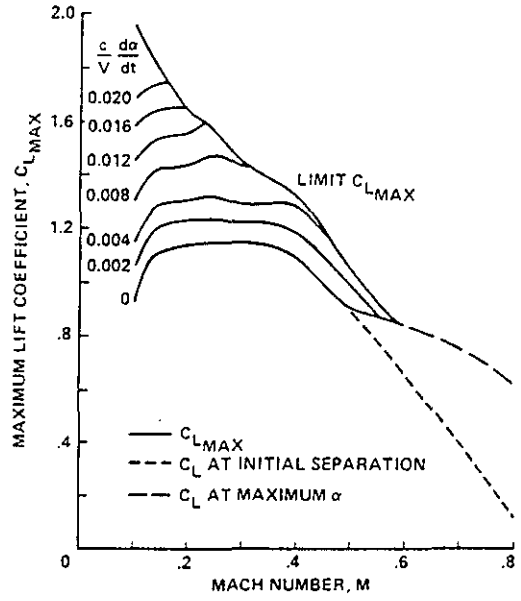

Figure 16. Maximum Pitching Rate Effect on LIft and Pitching-Moment Characteristics of Wing Model for Various Mach Numbers(from Reference 11).

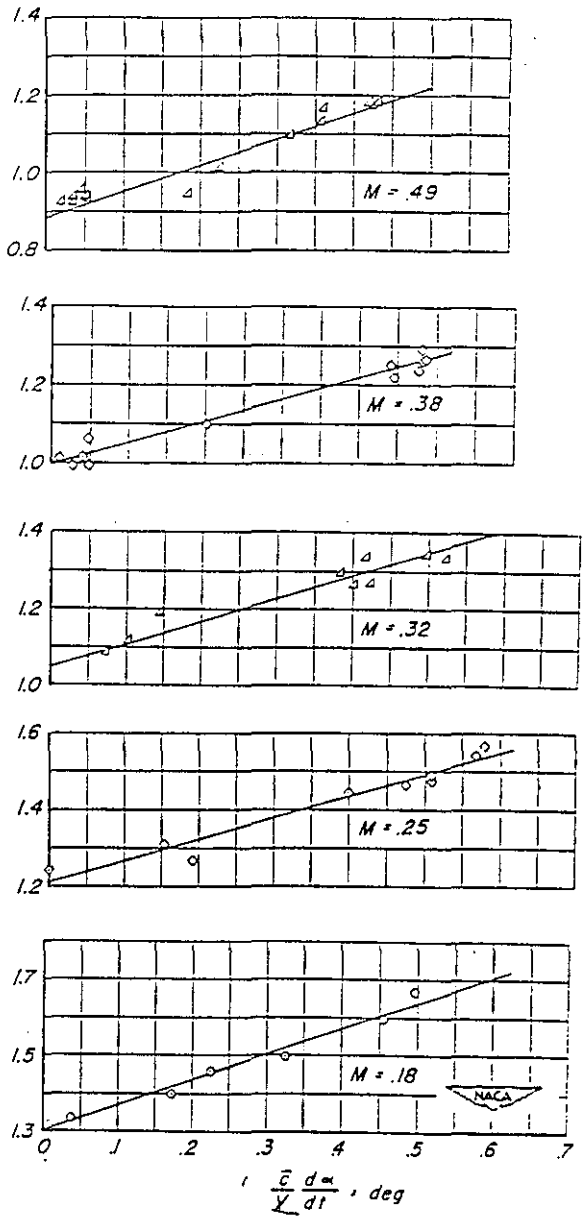

Figure 17. Maximum Attainable Lift Coefficient as a Function of Nondimensional Pitch Rates for an Aircraft Maneuvering at Various Mach Numbers(from Reference 12).

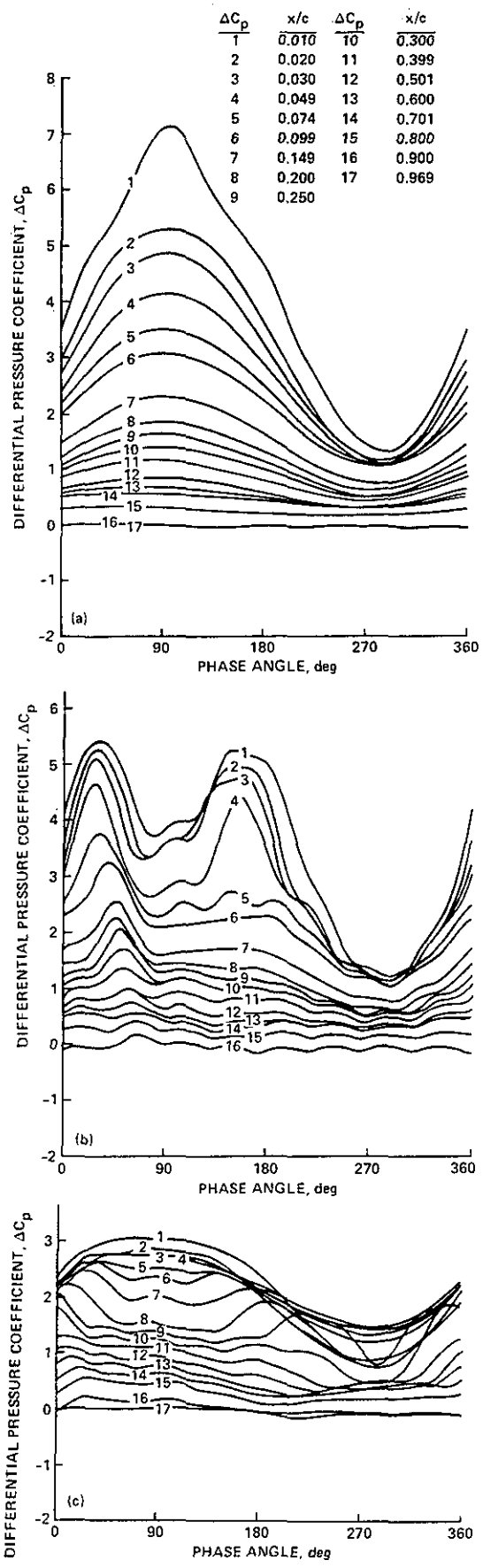

Figure 18. Instantaneous Pressure Distributions Measured on an Oscillating Airfoil at Different Free Stream Mach Numbers: (a) $M_\infty = 0.30$; (b) $M_\infty = 0.50$: (c) $M_\infty = 0.70$(from reference 13).

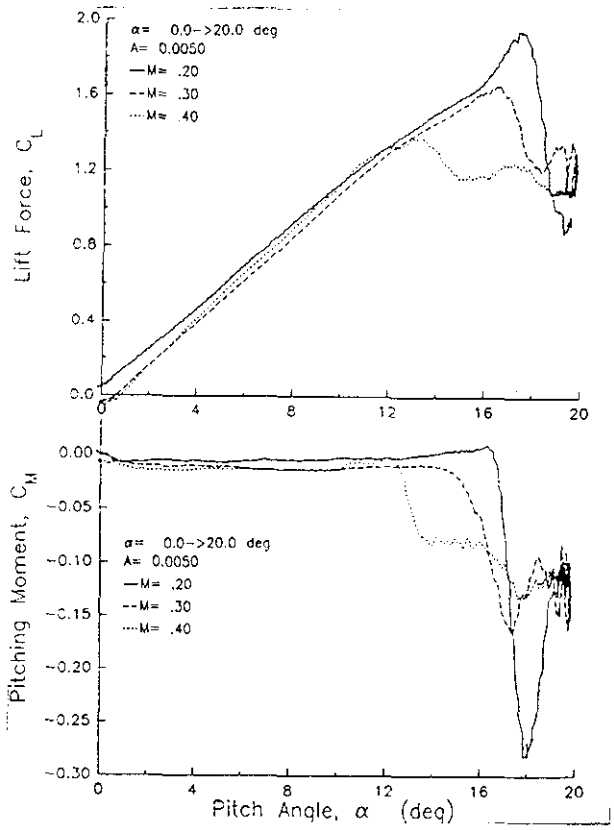

Figure 19. Effect of Free-Stream Mach Number on Lift and Pitching Moment of an Airfoil Experiencing Ramp Motion(from Reference 14).

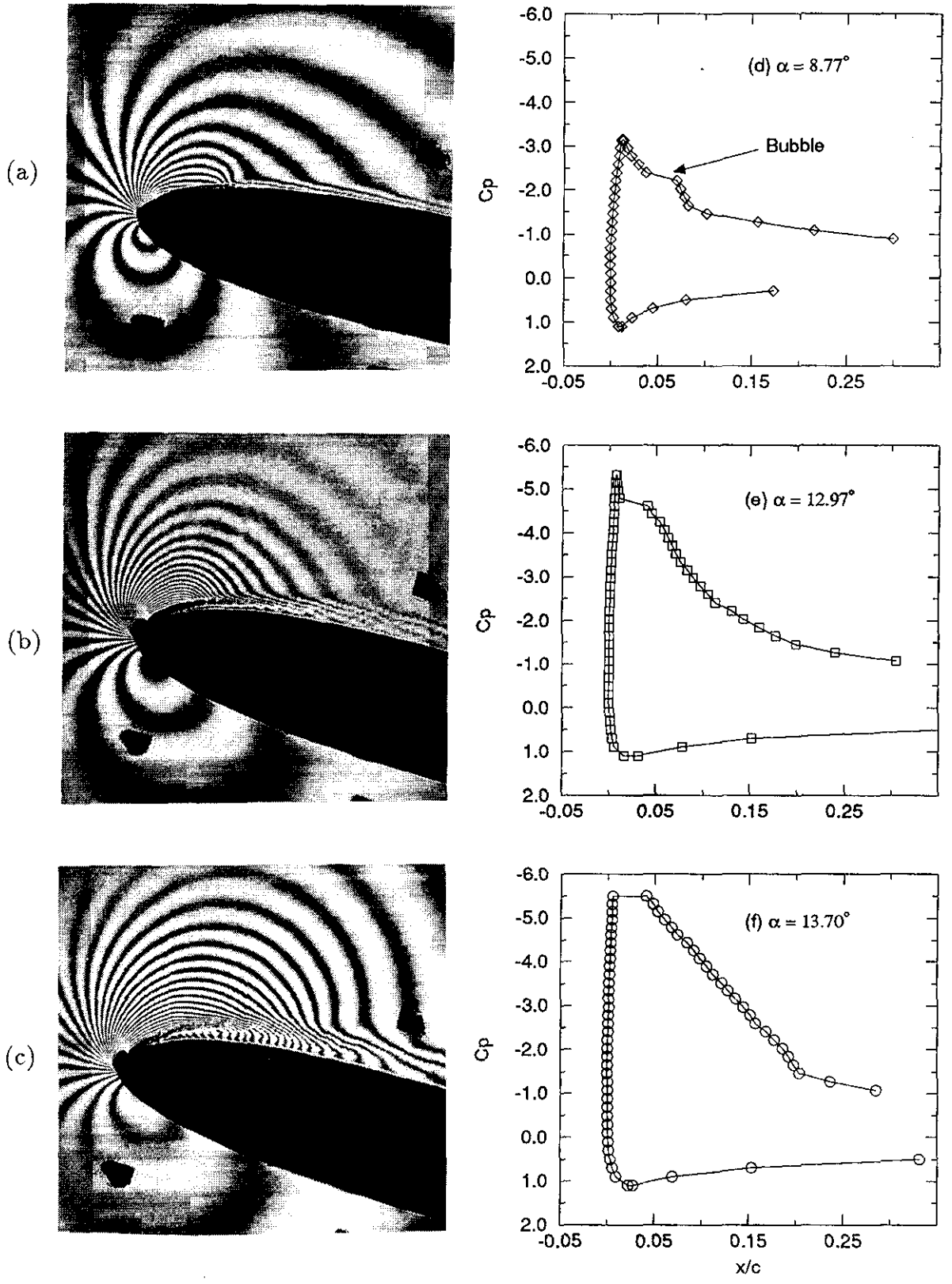

Figure 20. PDI Interferogram of Airfoil Oscillating in Pitch at $M_\infty = 0.30$, k = 0.075, and α= 10^o - 10^o sinωt, (a) $\alpha = 7.97^o$; (b) $\alpha = 12.48^o$; (c) $\alpha = 13.24^o$.

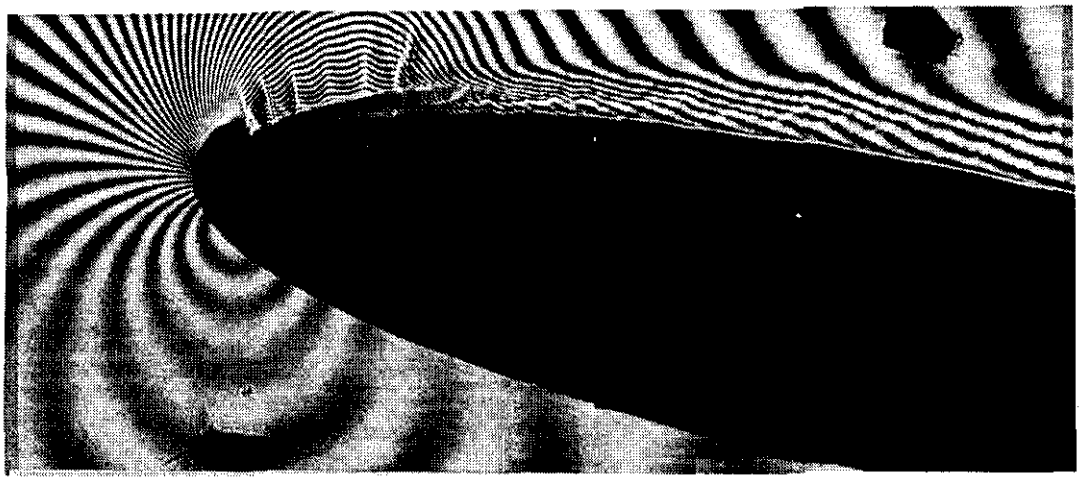

Figure 21. PDI Interferogram of Airfoil Showing Presence of Multiple Shocks at $M_\infty = 0.45$, k = 0.05, and $\alpha = 10°$(from Reference 18).

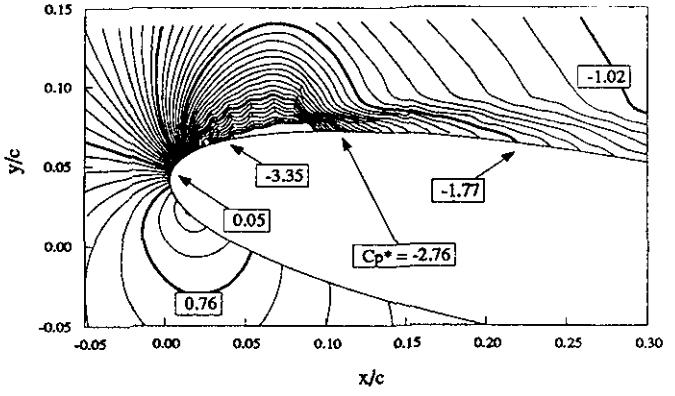

Figure 22. Global Pressure Coefficient Data for Airfoil Showing Presence of Multiple Shocks at $M_\infty = 0.45$, k = 0.05, and $\alpha = 10°$(from Reference 18).

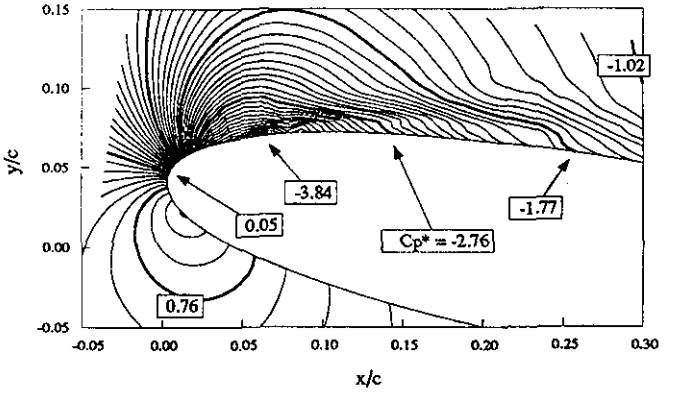

Figure 24. Global Pressure Coefficient Data for Oscillating Airfoil at $\alpha = 10.0°$, $M_\infty = 0.45$, Showing Presence of Two Shocks(from Reference 18).

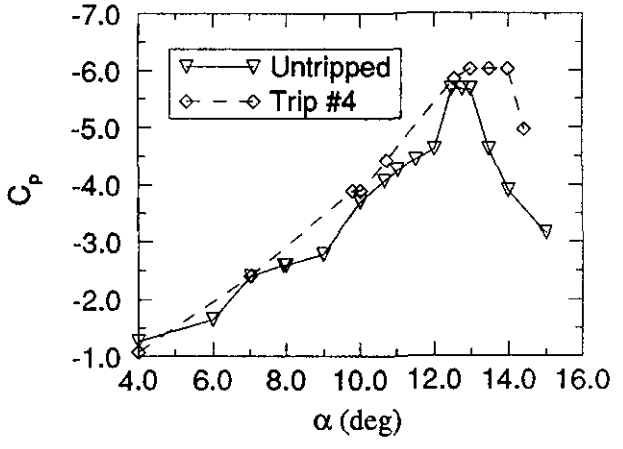

Figure 23. Development of Peak Suction as Function of Angle of Attack for Tripped and Untripped Airfoils at $M_\infty = 0.3$, k = 0.10(from Reference 18).

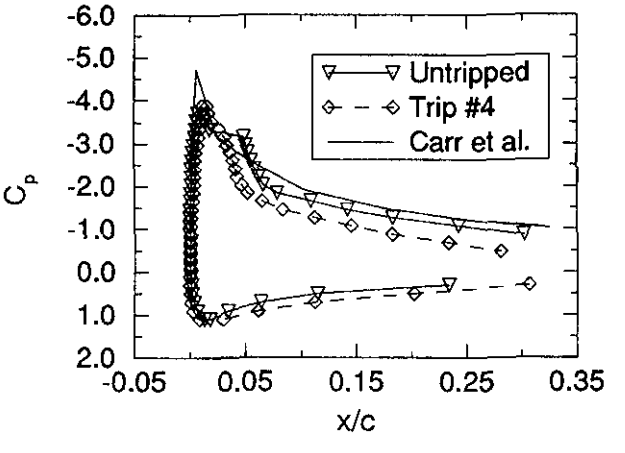

Figure 25. Comparison of Pressure Distributions Obtained at Model-Scale Reynolds Number with Experimental Results Obtained at $3x10^6$.

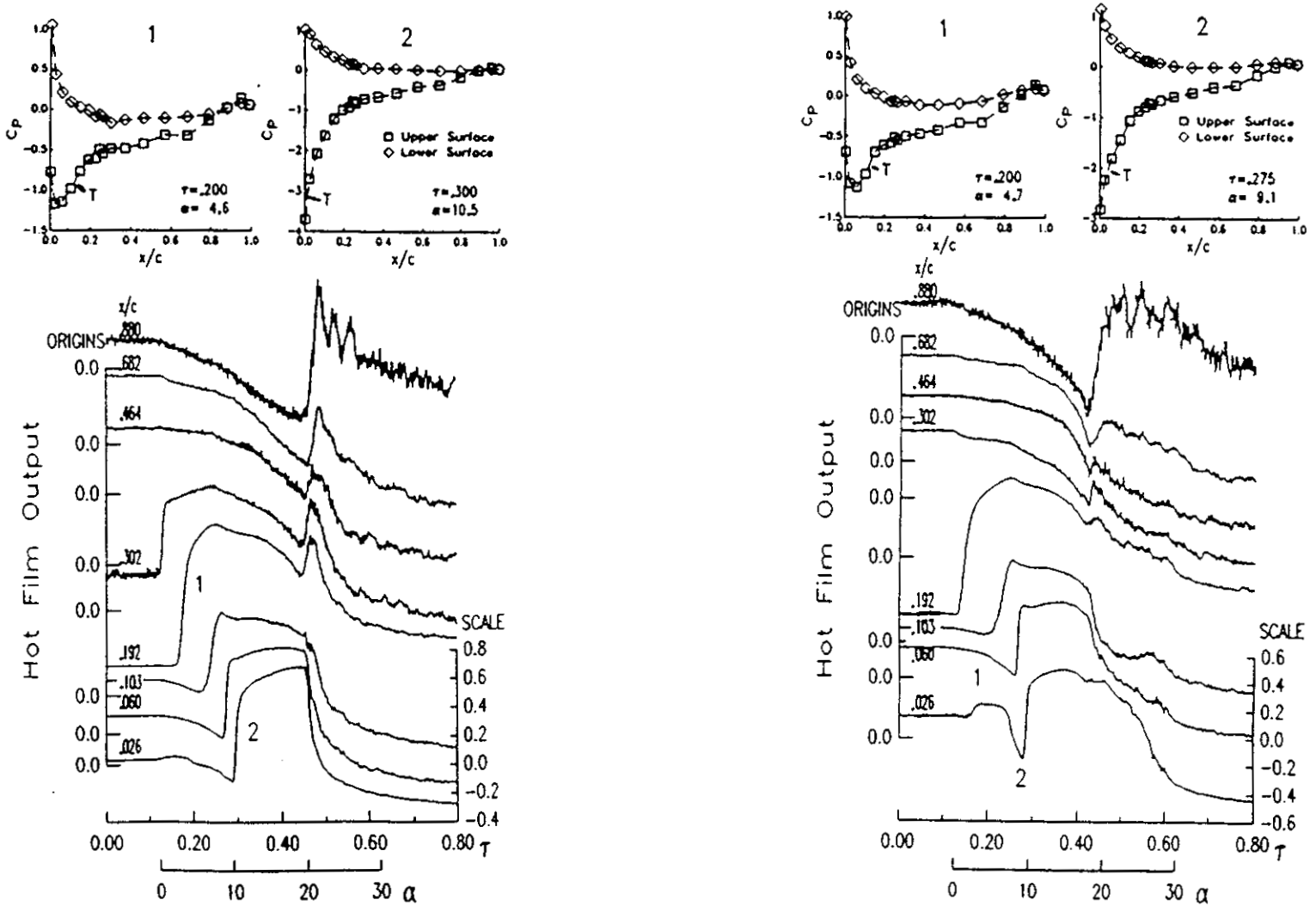

Figure 26. Instantaneous Surface Skin Friction and Pressure Distributions Obtained on An Airfoil Experiencing Ramp-Type Motion at High Reynolds Number, (a) $M_\infty = 0.20$; (b)$M_\infty = 0.30$(from Reference 19).

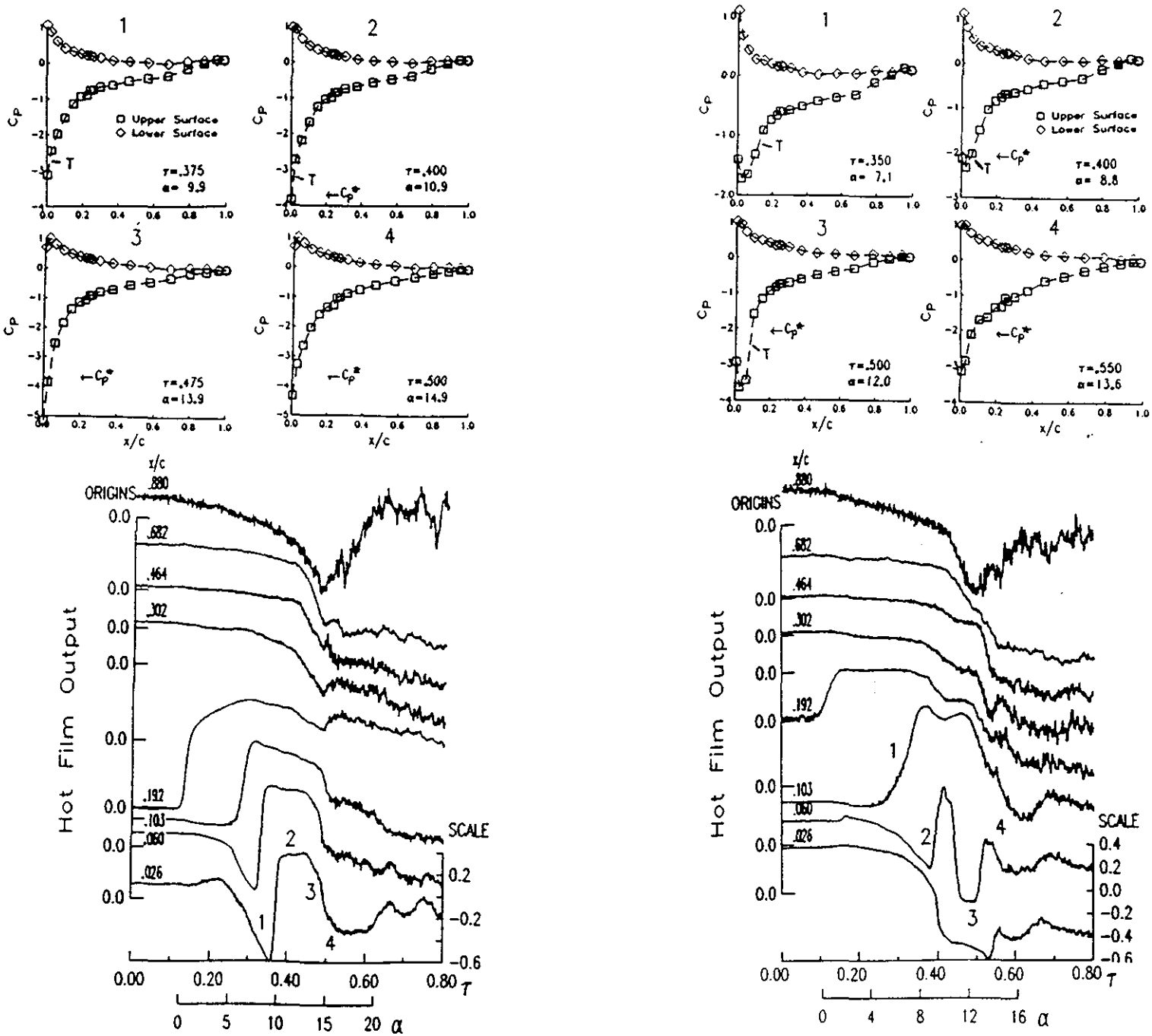

Figure 26(concluded). Instantaneous Surface Skin Friction and Pressure Distributions Obtained on An Airfoil Experiencing Ramp-T[illegible] Motion at High Reynolds Number. (c) $M_\infty = 0.40$; and (d)$M_\infty = 0.50$(from Referen[illegible]).

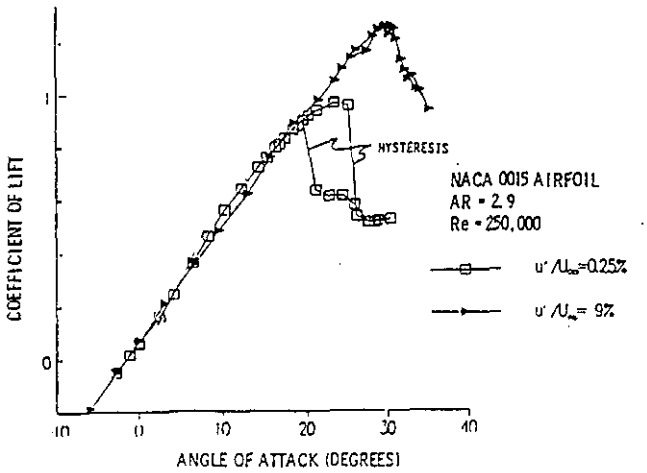

Figure 27. Effect of Free Stream Turbulence on Maximum Lift Coefficient of Low-Reynolds Number Airfoil(from Reference 22).

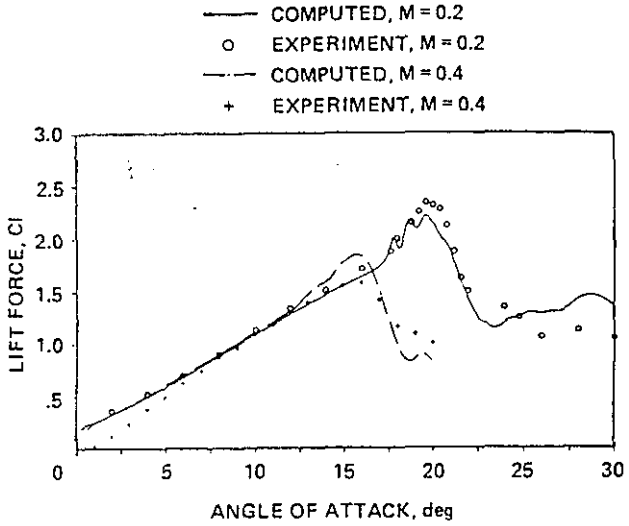

Figure 30. Computed Maximum Lift Coefficient as Function of Free-Stream Mach Number Compared to Experiment(from Reference 26).

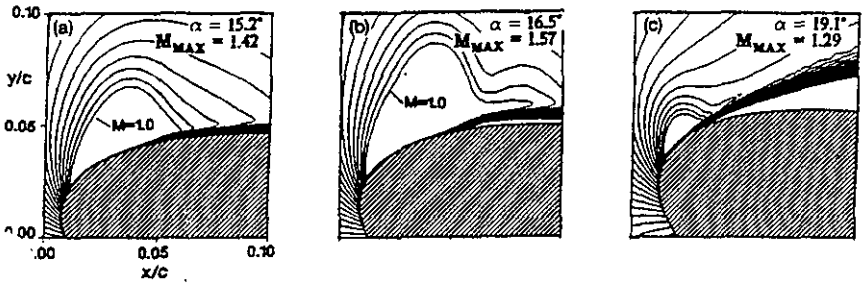

Figure 28. Development of Supersonic Region on Leading Edge of Airfoil During Dynamic Stall as Calculated Using Navier Stokes Equations, $M_\infty = 0.40$(from Reference 25).

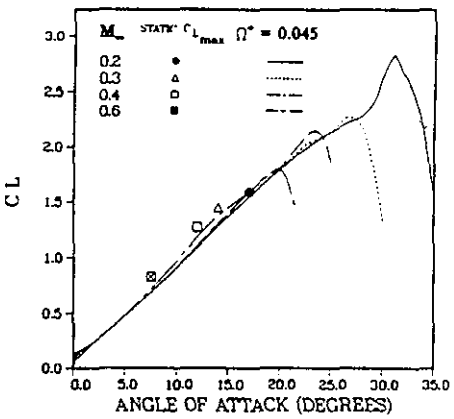

Figure 29. Calculated Maximum Lift Coefficient as Function of Free-Stream Mach Number(from Reference 26).